

An optimized absorbing potential for ultrafast, strong-field problems

Youliang Yu and B. D. Esry

J.R. Macdonald Laboratory, Kansas State University, Manhattan, Kansas, 66506

Theoretical treatments of strong-field physics have long relied on the numerical solution of the time-dependent Schrödinger equation. The most effective such treatments utilize a discrete spatial representation — a grid. Since most strong-field observables relate to the continuum portion of the wave function, the boundaries of the grid — which act as hard walls and thus cause reflection — can substantially impact the observables. Special care thus needs to be taken. While there exist a number of attempts to solve this problem — e.g., complex absorbing potentials and masking functions, exterior complex scaling, and coordinate scaling — none of them are completely satisfactory. The first of these is arguably the most popular, but it consumes a substantial fraction of the computing resources in any given calculation. Worse, this fraction grows with the dimensionality of the problem. And, no systematic way to design such a potential has been used in the strong-field community. In this work, we address these issues and find a much better solution. By comparing with previous widely used absorbing potentials, we find a factor of 3–4 reduction in the absorption range, given the same level of absorption over a specified energy interval.

I. INTRODUCTION

To theoretically describe highly nonperturbative interactions — such as strong-field physics — in a fully quantitative manner, the best option is usually to numerically solve the time-dependent Schrödinger equation (TDSE). One of the most popular approaches to practically solving the TDSE represents the wave function on a finite spatial grid with boundary conditions applied at its edges. In general, such a grid needs to be large enough so that there are no reflections from the boundaries which behave as infinitely hard walls. Otherwise, the reflections might lead to unphysical changes in the observables. For example, an ionized wavepacket reflected from the boundary back to the origin might be driven by the laser field into bound states, thus reducing the total ionization yield.

The most direct way to avoid such spurious reflections is to move the boundary further away. Since the grid density is fixed physically by the highest energy, however, this requires more grid points which, in turn, incurs a greater computational cost. In fact, the large grids required to describe current experiments have become a key bottleneck to improving the numerical efficiency of solving the TDSE, especially as laser wavelengths push beyond 800 nm.

Fortunately, if the wave function at large distances can easily be reconstructed or is not of interest, it can be absorbed at a sufficiently large distance that it does not affect the dynamics at small distances. Applying such absorption techniques, one can generally reduce the box size significantly. The absorb-and-reconstruct strategy was probably first developed by Heather and Metiu [1] which they demonstrated for strong-field dissociation. Their work has been adopted in hundreds of papers since. A new implementation following this philosophy [2, 3] has proven similarly effective.

Among the various methods to effect absorption at the boundary, the most widely used — and probably the simplest — method is the complex absorbing potential (CAP) [4–17] or the closely related masking function [18].

Another increasingly popular absorbing-boundary technique is exterior complex scaling [19–23], where one rotates the coordinate into the complex plane at large distances. Other, less common, methods to treat the boundary reflection include time-dependent coordinate scaling [24–26], the interaction representation [27–29], and Siegert-state expansions [30]. While these methods are local in time and vary from exact to approximate, it is also possible to construct a perfectly transparent boundary using Feshbach projection techniques [13]. The disadvantage of such methods is that they require the wave function from previous times and are thus nonlocal in time. In this work, we will focus on the CAP due to its popularity and the simplicity of its implementation. Our goals are to make it both more efficient and more effective.

Although the CAPs utilized in previous studies are predominantly polynomials [8, 9, 12–14, 16, 17], other types of absorbing potentials such as \cos^2 [15], Pöschl-Teller ($1/\cosh^2$) [4], and a pseudo-exponential [$\exp(-x^{-n})$] [5, 6] have also been used. In most of these papers, the CAP's performance is examined by studying the dependence of the reflection R and transmission T coefficients on the energy. Riss and Meyer [8], for instance, carefully investigated the properties of R and T for polynomial CAPs, finding some difficulty in treating low energies. They characterized their optimized potential parameters in terms of the absorbed energy ratio E_{\max}/E_{\min} , where E_{\min} and E_{\max} indicate the minimum and maximum energies, respectively, for which absorption exceeds a given value. The maximum ratio they considered, 30, is too small, however, for typical strong-field electronic dynamics. We will, for instance, consider $E_{\max}/E_{\min}=500$. Vibok and Balint-Kurti [5, 6] presented a more optimal CAP — the $\exp(-x^{-n})$ type — for heavy particles, but the range of absorbed energies was still insufficient for strong-field problems.

Even though R and T provide a clear, quantitative measure of performance, studies of CAPs in strong-field problems utilizing them can hardly be found. Their ab-

TABLE I. The CAPs considered in this work, both from the literature and proposed in this work.

CAP type	$V(x)$ (units of $\hbar^2/2m$)
quadratic [8, 13]	$-i\alpha^2(x-x_0)^2$
cosine masking function [18]	$-i\alpha^2 \log\{\sec[(x_0-x)/\beta]\}$
M-JWKB [11]	$-ik_{\min}^2 \epsilon(x)$
quartic [8, 13]	$-i\alpha^2(x-x_0)^4$
pseudo-exponential [5]	$-i\alpha^2 e^{-\beta/(x_0-x)}$
Pöschl-Teller [4]	$-i\alpha^2 \operatorname{sech}^2[(x+x_0)/\beta]$
single-exponential (present)	$-\alpha^2 e^{-x/\beta}$
double-exponential (present)	$-\alpha_1^2 e^{-x/(2\beta)} - i\alpha_2^2 e^{-x/\beta}$
double-sinh (present)	$-\alpha_1^2/(2 \sinh[x/(2\beta)])$ $-i\alpha_2^2/(2 \sinh[x/(2\beta)])^2$

sence is likely due to the inherent time-dependent nature of the strong-field problem and the authors' consequent focus on wavepacket behavior, losing track of the connection with R and T . In contrast, we will adopt R as the figure of merit for designing our absorbing potentials for the strong-field problem, incorporating it as a critical piece in our systematic CAP construction method.

The major advantage of the CAP is its simplicity. The major disadvantage is that it has required a relatively large spatial range to be effective, thus consuming non-negligible computational resources. In this paper, we improve the performance of the CAP and systematically design a more optimal — yet general — CAP for strong-field processes. Specifically, we provide an optimized CAP with a factor of 3–4 reduction in the absorption range compared to some widely-used CAPs [13]. Our optimized CAP absorbs at a prescribed level over a large enough energy range to be useful for strong-field processes.

To be clear, while we optimize our CAP for the strong-field problem, it can be readily adapted and re-optimized for other problems following the procedures we outline below.

II. THEORETICAL BACKGROUND

Since a time-dependent wavepacket can always be written as a superposition of the time-independent scattering states, we use the time-independent reflection coefficient as a quantitative tool for characterizing and designing an optimal CAP. We will require the CAP's reflection coefficient to remain below a cutoff value R_c , $R \leq R_c$, over a given energy range $E_{\min} \leq E \leq E_{\max}$. Since the spatial region devoted to the CAP near the edge of the grid is unphysical, we wish to minimize the computing resources it consumes as much as possible. Therefore, in this work, our optimization efforts focus on reducing the absorption range x_R , as defined in Fig. 1, while meeting the absorption criteria above.

We study one-dimensional CAPs since they can be easily adapted to higher dimensions, obtaining the reflection

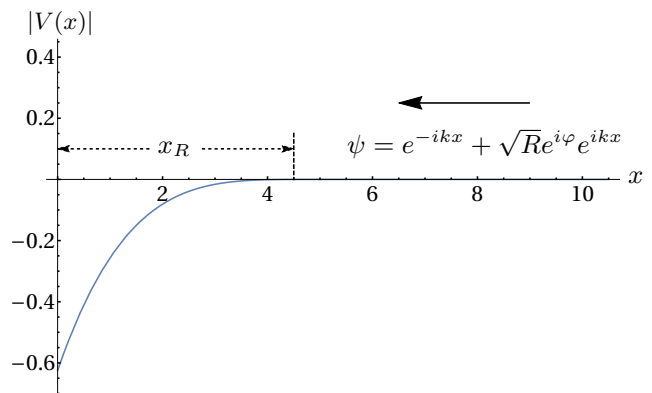


FIG. 1. The scheme used to characterize a CAP and determine its reflection coefficient. The edge of the grid is taken to be $x = 0$, and we require $\psi(x=0) = 0$ as is typical in solving the TDSE. We assume incidence from the right as indicated. We define the absorption range x_R from the distance at which the absorbing potential decreases beyond a cutoff value V_c and can be neglected, $|V(x_R)| = V_c$.

coefficient R by solving the Schrödinger equation,

$$\left[-\frac{\hbar^2}{2m} \frac{d^2}{dx^2} + V(x)\right] \psi = E\psi, \quad (1)$$

as indicated schematically in Fig. 1. We consider the potential $V(x)$ to be one of the CAPs listed in Table I. The shapes of all the CAPs considered are generically as in Fig. 1 and are controlled by the following parameters: α^2 is the strength of the potential, β mainly determines its width, and x_0 is a shift. These are the parameters that will be varied to optimize the CAPs.

The JWKB-based CAP obtained by Manolopoulos [11] — labeled M-JWKB in Table I — is qualitatively different from the others, however, in that it requires no optimization. This simplicity is certainly one of its strengths and derives from the fact that its reflection coefficient effectively decreases monotonically from unity at zero energy to $e^{-\sqrt{2}\pi/\delta}$ at infinite energy. Its explicit expression is in terms of the Jacobi elliptic function $\operatorname{cn}(u, k)$,

$$\epsilon(x) = \sqrt{\operatorname{cn}^{-4}[2\delta k_{\min}(x_0-x)/\sqrt{2}, 1/\sqrt{2}] - 1}, \quad (2)$$

with $x_0 = 2.622/(2\delta k_{\min})$ where $k_{\min} = \sqrt{2mE_{\min}/\hbar^2}$ [11]. One simply chooses δ from the condition $R(E_{\min}) = R_c$.

The first five CAPs in the table are defined to be non-zero only for $0 \leq x \leq x_0$ and to vanish identically for $x > x_0$. The remaining CAPs are defined for all x , but vanish exponentially with x . The first four CAPs are some of the most commonly used, with the cosine masking function recast as a CAP using $e^{-iV(x)\Delta t} \sim \cos^{1/8}[(x-x_0)/\beta]$.

We include the Pöschl-Teller potential because it is well known to be reflectionless for specific *real* values of $i\alpha^2$, suggesting that it might have advantageous properties as a CAP. It can be shown analytically, however,

that this property no longer holds for complex $i\alpha^2$. In the process of optimizing it for the present purposes, we found that shifting its center off the grid minimized x_R , leaving only its exponential tail on the grid. This result suggested using instead the simpler family of exponential CAPs included in the table.

We calculate the reflection coefficient numerically using the finite-element discrete-variable representation (FEDVR) [31, 32] and eigenchannel R-matrix method [33]. The reflection coefficient can also be calculated analytically for several of the potentials in Table I. However, we give the analytic solutions (derivations in the appendices) only for the CAPs we propose—namely, the single-exponential and double-exponential CAPs. The double-sinh potential has no analytic solution to the best of our knowledge. In these cases, we confirmed that the R-matrix reflection coefficients agreed with the analytical R to several significant digits.

Since our primary goal is to systematically design an absorbing potential for the strong-field ionization problem with predetermined properties, we will use atomic units for the remainder of our discussion. Our results can be readily applied to other problems, though, using the derivations in the appendices in which the masses and SI units are explicitly retained.

III. OPTIMIZATION OF PROPOSED CAPS

We demonstrate our optimization procedure in detail below first for the single-exponential CAP since it is the simplest to optimize. It also establishes a few key results important for the optimization of our recommended CAPs: the double-exponential and double-sinh potentials. Whether the solution is analytical or numerical, the procedure we describe for optimization is the same and can be applied to other CAPs as well. In fact, this is what we have done for the comparison in Sec. IV.

The values of R_c , E_{\min} , and E_{\max} that we will focus on for this discussion are

$$R_c = 10^{-3}, \quad E_{\min} = 0.006 \text{ a.u.}, \quad \text{and} \quad E_{\max} = 3 \text{ a.u.} \quad (3)$$

We chose this energy range to cover $0.1\hbar\omega \leq E \leq 14U_p$ for an 800-nm laser pulse at 10^{14} W/cm^2 (U_p is the pondermotive energy: $U_p = I/4\omega^2$ with I the intensity and ω the laser frequency). This energy range includes essentially all photoelectrons one would expect to be produced in this typical pulse. In momentum, which is more convenient for the analytical R , this range corresponds to

$$k_{\min} = 0.110 \text{ a.u.} \quad \text{and} \quad k_{\max} = 2.45 \text{ a.u.} \quad (4)$$

Note that $14U_p$ exceeds the highest-energy electrons one would normally expect in a strong-field problem, but we will show below that this choice has little effect on the resulting x_R . Finally, we use $V_c=10^{-4} \text{ a.u.}$ to define x_R from $|V(x_R)|=V_c$.

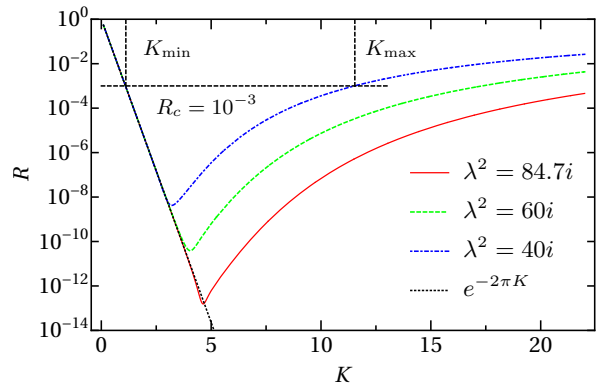


FIG. 2. Examples of the reflection coefficient $R(K)$ for a single-exponential CAP with different potential strengths. The predicted small- K behavior, $e^{-2\pi K}$, is shown for comparison. The unitless limits K_{\min} and K_{\max} for which $R(K) \leq R_c$ holds are also indicated.

A. Single-Exponential CAP

We take the single-exponential CAP to have the form

$$V(x) = -\frac{\hbar^2 \alpha^2}{2m} e^{-x/\beta} \quad (5)$$

Its reflection coefficient, as shown in App. A, is

$$R = e^{4K \arg \lambda^2} \left| \frac{J_{2iK}(2\lambda)}{J_{-2iK}(2\lambda)} \right|^2, \quad (6)$$

where the unitless momentum is $K = k\beta$ with $k = \sqrt{2E}$ and the unitless potential strength is $\lambda = \alpha\beta$. To achieve our goal of minimizing x_R , we must find the optimal λ and β .

1. Purely imaginary potential

For a purely imaginary potential, $\lambda^2 \propto i$, Fig. 2 shows the behavior of R as a function of K . As the figure suggests, one can show from Eq. (6) that

$$R \xrightarrow{K \rightarrow 0} e^{-2\pi K}. \quad (7)$$

As can also be seen in the figure, increasing the strength $|\lambda^2|$ of the CAP means this exponential decrease continues to larger K and the large- K tail decreases.

We can thus use Eq. (7) to write

$$K_{\min} = -\frac{1}{2\pi} \log R_c, \quad (8)$$

giving

$$K_{\min} = 1.10$$

for $R_c = 10^{-3}$. From $K_{\min} = k_{\min}\beta$, the scale β is therefore determined:

$$\beta = \frac{K_{\min}}{k_{\min}} = 10.0 \text{ a.u.}$$

We can now find the required λ^2 from

$$R(K_{\max}) = R\left(\frac{k_{\max}}{k_{\min}}K_{\min}\right) = R_c \quad (9)$$

since $K_{\max}=k_{\max}\beta$. Solving this equation gives

$$\lambda^2 = 84.7i \text{ and } x_R = 83.4 \text{ a.u.} \quad (10)$$

This example illustrates the fact that x_R can only be substantially decreased if β is decreased. Thus, K_{\min} and k_{\min} determine x_R , and K_{\min} is set by the form of the CAP and its parameters. In general, the smaller k_{\min} is, the more difficult absorption becomes. Roughly speaking, this behavior can be traced to the need for x_R to be large enough for the potential to contain the longest wavelength to be absorbed.

2. Complex potential

Given k_{\min} , decreasing β further requires decreasing K_{\min} . This is not possible with a purely imaginary single-exponential CAP, so we must allow λ^2 to be complex.

The reflection coefficient in Eq. (6) still holds for complex λ^2 and looks generically like those displayed in Fig. 2 — with the exception that

$$R \xrightarrow[K \rightarrow 0]{} e^{-4\pi K + 4K \arg \lambda^2}. \quad (11)$$

This small- K behavior suggests that the best way to reduce K_{\min} — and thus β and x_R — is to make $\arg \lambda^2$ small (since $\arg \lambda^2$ must be positive to have absorption). That is, we should make $\text{Re } \lambda^2$ much larger than $\text{Im } \lambda^2$. The fastest decay one can achieve with this approach is $e^{-4\pi K}$ which, in turn, sets the limit on how small K_{\min} can be.

The physical origin of this faster low- K decrease is clear: the real part of the potential is attractive and accelerates the wave before it encounters the imaginary part of the potential [13]. Absorption thus occurs at a shorter wavelength where absorption can be efficient with a much smaller x_R . Since $\text{Im } \lambda^2$ must be large enough for sufficient absorption, however, $\arg \lambda^2$ cannot be zero. The optimum value will be a compromise between these two factors.

To determine the magnitude of the improvement in x_R , we use $\lambda = |\lambda|e^{i\chi}$ and the small- K behavior in Eq. (11) to write

$$K_{\min} = \frac{\log R_c}{4(2\chi - \pi)}. \quad (12)$$

From this, we can find β and K_{\max} for a given χ . Combining everything and simplifying reduces the problem to solving Eq. (9) for $|\lambda|$ with $R(K)$ from Eq. (6). The resulting x_R as a function of χ is shown in Fig. 3.

The figure shows that the optimization problem has been reduced to a one-dimensional minimization of x_R with respect to χ . As expected, the solution,

$$x_R = 57.1 \text{ a.u.} \quad (13)$$

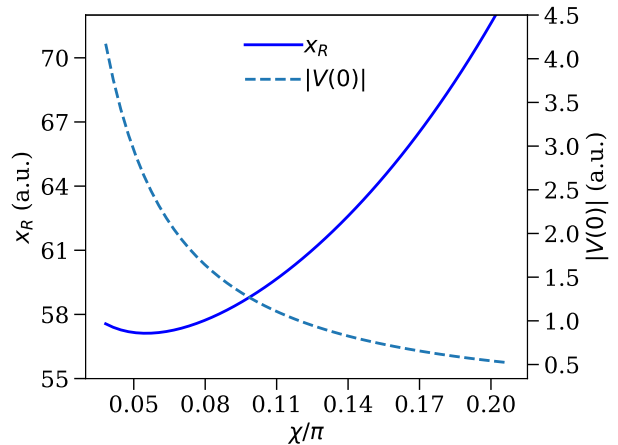


FIG. 3. Absorption range and potential depth for a single-exponential CAP, showing their dependence on the complex phase of λ . The magnitude of λ is determined at each χ by solving Eq. (9).

at $\chi=0.055\pi$ (with $|\lambda^2| = 165$), lies at small χ . Adding a real part to the absorbing potential has thus reduced the absorption range by 32% over the purely imaginary single-exponential CAP.

Figure 3 also shows that at the optimal x_R , the potential is 2.62 a.u. deep. This is roughly equal to E_{\max} , leading to local kinetic energies of approximately $2E_{\max}$ and thus requiring a much denser spatial grid in the absorption region. Guided by the figure, however, we see that a modest few-percent increase in x_R to 58.9 a.u. ($\lambda^2 = 97e^{i\pi/5}$) reduces $|V(0)|$ to 1.25 a.u., making it more computationally attractive. Further reduction in $|V(0)|$ can, of course, be achieved — at the expense of x_R .

Figure 4 shows the optimum R for both the purely imaginary single-exponential CAP of the previous section and the complex single-exponential CAP of the present section. The coefficients satisfy $R \leq R_c$ for different ranges of the scaled momentum K but the same range of the physical momentum k . The range of K covered by the complex CAP is smaller than for the imaginary CAP by the ratio of their respective K_{\min} 's.

B. Double-Exponential CAP

It has long been known, of course, that adding a real potential improves CAP performance [13]. And, given the improvement to the single-exponential CAP afforded by doing so, it is natural to ask whether we can do even better with a more flexible complex potential.

Since we want to retain the ability to calculate R analytically and since the real part must have longer range than the imaginary part, we choose the CAP to be

$$V(x) = -\frac{\hbar^2\alpha_1^2}{2m}e^{-x/2\beta} - i\frac{\hbar^2\alpha_2^2}{2m}e^{-x/\beta}. \quad (14)$$

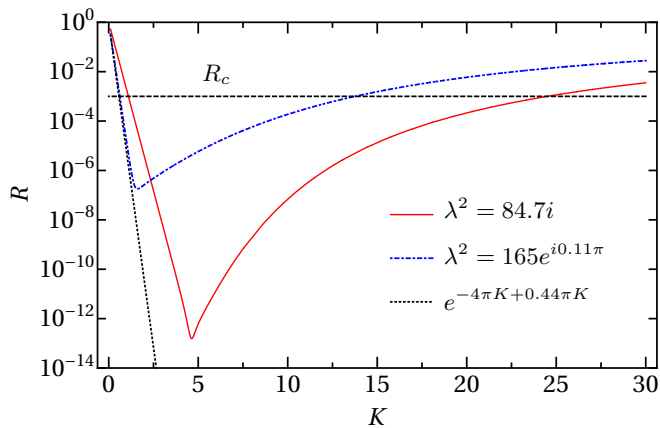


FIG. 4. The optimum reflection coefficients for purely imaginary and complex single-exponential CAPs as a function of the unitless momentum.

The reflection coefficient, as shown in App. B, can be written in terms of the confluent hypergeometric function as

$$R = \left| \frac{{}_1F_1(\eta + 2iK, 1 + 4iK, -4\gamma^3\lambda_2)}{{}_1F_1(\eta - 2iK, 1 - 4iK, -4\gamma^3\lambda_2)} \right|^2 \quad (15)$$

where

$$\begin{aligned} K &= k\beta & \lambda_1 &= \alpha_1\beta & \lambda_2 &= \alpha_2\beta \\ \gamma &= e^{i\pi/4} & \Lambda &= \frac{\lambda_1^2}{\lambda_2} & \eta &= \frac{1}{2} - \gamma\Lambda. \end{aligned}$$

1. λ_1 and λ_2 independent

Given the extra potential parameter, optimizing the double-exponential CAP is clearly more challenging than for the single-exponential CAP. And, the complicated expression for R only exacerbates the task. It would therefore be convenient to find a regime in which λ_1 and λ_2 are independent since this would greatly simplify the optimization.

To this end, we show in Fig. 5 the dependence of R on λ_1 and λ_2 . Generally speaking, λ_1 — the coefficient of the longer-ranged, real part of V — controls the low-energy behavior, while λ_2 — the coefficient of the shorter-ranged, imaginary part of V — controls the high-energy behavior. The underlying physical reasons for these connections are the same as discussed for the single-exponential CAP.

Figure 5 also shows that for λ_1 and λ_2 large enough,

$$R \rightarrow e^{-8\pi K} \quad (16)$$

for $R \sim R_c$. This behavior immediately shows the benefit of the double exponential since it falls faster than is possible with a single exponential, Eq. (11), leading to a smaller K_{\min} and thus a smaller x_R .

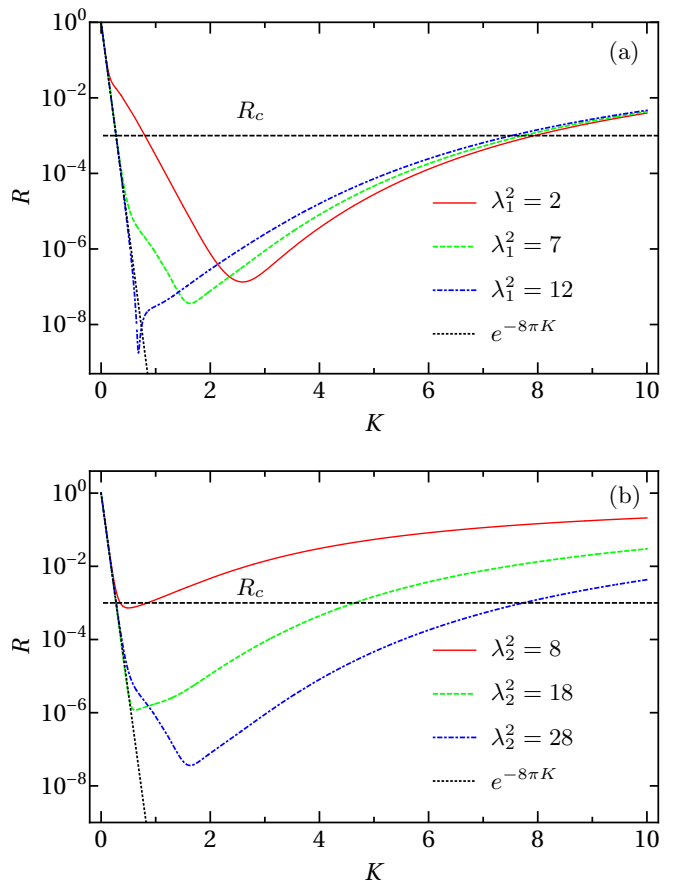


FIG. 5. Illustration of the dependence of R for a double-exponential CAP on the potential strength: (a) λ_1 dependence for $\lambda_2^2 = 28$, and (b) λ_2 dependence for $\lambda_1^2 = 7$.

In the regime that Eq. (16) holds, K_{\min} is independent of λ_1 and λ_2 and takes the value

$$K_{\min} = -\frac{1}{8\pi} \log R_c. \quad (17)$$

For $R_c=10^{-3}$, $K_{\min}=0.275$ which is indeed much smaller than was possible with the single-exponential CAP.

Minimizing x_R now requires fixing λ_1 to a large enough value that Eq. (16) holds ($\lambda_1^2 \gtrsim 6$ is typically sufficient) and solving Eq. (9) for λ_2 . Using R from Eq. (15) and $K_{\max}=6.125$, we find, for instance,

$$\lambda_1^2 = 6 \text{ and } \lambda_2^2 = 22.6, \text{ leading to } x_R = 42.4 \text{ a.u.} \quad (18)$$

and the reflection coefficient shown in Fig. 6. There are, however, any number of combinations of λ_1 and λ_2 that satisfy Eq. (9). Since x_R for the double-exponential CAP is determined to a very good approximation by λ_1 alone, though, one would typically choose the smallest possible λ_1 to obtain the smallest possible x_R . At the same time, it should be noted that $x_R \propto \log \lambda_1$, so it is not terribly sensitive to small changes in λ_1 . Choosing the smallest λ_1 , however, also ensures that $|V(0)|$ is minimized, thereby keeping the numerical cost down.

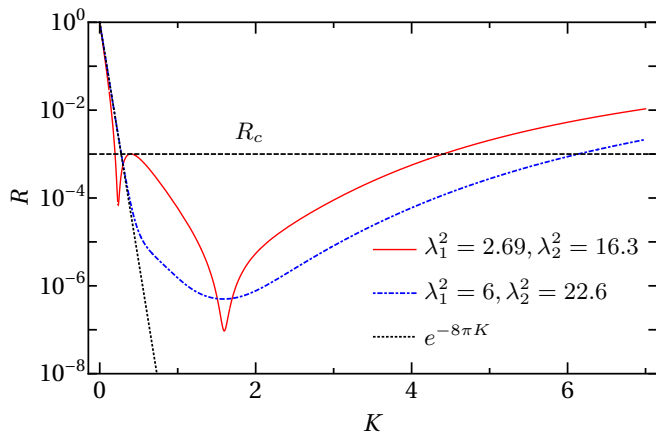


FIG. 6. The optimum reflection coefficient as a function of the unitless momentum for the double-exponential CAP with λ_1 and λ_2 both independent and not independent.

2. λ_1 and λ_2 not independent

Although $x_R=42.4$ a.u. is a significant improvement over the single-exponential result, $x_R=57.1$ a.u., we can do better. The way to do this is to consider smaller λ_1^2 where there are particular combinations of λ_1 and λ_2 for which R falls off faster than Eq. (16). Such behavior permits smaller K_{\min} and thus smaller x_R . Of course, λ_1 and λ_2 are no longer independent in this regime, but it is still true that λ_1 largely—but not as completely as above—controls K_{\min} and λ_2 , K_{\max} .

Figure 6 illustrates the small- K behavior that we want to take advantage of. For this combination of λ_1 and λ_2 , R dips below the exponential from Eq. (16) for $R \sim R_c$ as seen in the figure. At this and other such parameter combinations, a local minimum develops in R at K near K_{\min} as shown in the figure. In practice, one searches for these λ_i combinations to minimize K_{\min} while simultaneously ensuring that the local maximum in R remains below R_c .

To find the minimum value of K_{\min} , we take advantage of its weak dependence on λ_2 by first minimizing with respect to λ_1 for some reasonable choice of λ_2 . With this value of λ_1 , we then solve Eq. (9) for λ_2 . Since there is a weak dependence on λ_2 , though, K_{\min} must be re-minimized for λ_1 with this new λ_2 . Then, Eq. (9) must again be solved and the iteration continued until sufficient convergence in λ_1 and λ_2 is obtained. Typically, only a handful of iterations are necessary to find 3 digits. More sophisticated methods of performing the constrained minimization of $x_R(\lambda_1, \lambda_2)$ could, of course, be employed as well.

As above, there are many combinations of λ_1 and λ_2 that give the smallest K_{\min} , $K_{\min} = 0.197$. But, our ultimate goal of minimizing x_R leads us to choose the smallest λ_1 possible. One convenient example for the

optimal values is

$$\lambda_1^2 = 2.69 \text{ and } \lambda_2^2 = 16.3,$$

which leads to

$$\beta = 1.79 \text{ a.u. and } x_R = 29.9 \text{ a.u..}$$

The corresponding R is shown in Fig. 6. Although difficult to prove, this choice appears to be the global optimum for this choice of E_{\min} , E_{\max} , and R_c .

C. Double-sinh CAP

While straightforward, the optimization procedure outlined above for achieving such a substantial reduction in x_R is somewhat tedious. Fortunately, it needs to be done only once for a given R_c and ratio E_{\max}/E_{\min} . Should one wish to change R_c or only one of the energy limits, however, re-optimization is required. It turns out, though, that the latter limitation can be lifted without compromising on x_R .

In general, one expects the reflection coefficient to be unity for $E = 0$ and $E \rightarrow \infty$, and this is the behavior displayed by all the reflection coefficients we have shown. Consequently, the reflection coefficient necessarily satisfies $R(E) = R_c$ at both low and high energies. As mentioned in Sec. II, however, the M-JWKB CAP [11] produces an R that decreases more-or-less monotonically to a value controllably less than unity at infinite energy. Its parameters thus do not depend on E_{\max} , removing the need for re-optimizing with changes in either E_{\min} or E_{\max} . Unfortunately, x_R for the M-JWKB CAP turns out to be 118 a.u. because its R falls off relatively slowly at low energies, leading to a large K_{\min} .

To retain both the small x_R found for the double-exponential CAP and the advantageous high-energy behavior of the M-JWKB CAP, we have designed the double-sinh CAP:

$$V(x) = -\frac{\hbar^2}{2m} \frac{\alpha_1^2}{2 \sinh \frac{x}{2\beta}} - i \frac{\hbar^2}{2m} \frac{\alpha_2^2}{4 \sinh^2 \frac{x}{2\beta}}. \quad (19)$$

At large distances, this CAP reduces exactly to the double-exponential CAP, thus possessing its nice long-wavelength, low-energy properties. At short distances, this CAP is dominated by the $-i\alpha_2^2/x^2$ divergence of the second term. It is this behavior that is inspired by the M-JWKB CAP and that leads to similarly desirable high-energy behavior.

Unlike the single- and double-exponential CAPs, R for the double-sinh potential is not analytic as far as we know (unless $\alpha_1=0$ —in which case, it reduces to one-half of the generalized Pöschl-Teller potential [34]). We must thus calculate R numerically, and the optimal result is shown in Fig. 7 along with the optimal double-exponential result for comparison. Their absorption ranges are $x_R=28.8$ a.u. and $x_R=29.9$ a.u., respectively, confirming that there is no compromise on x_R . We

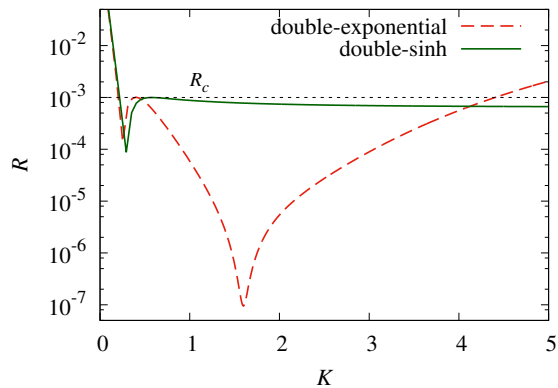


FIG. 7. Optimal R for the double-sinh CAP along with the optimal R for the double-exponential CAP for comparison using parameters in Table II, both as a function of the unitless momentum.

note that the qualitative behavior of the double-sinh R shown is typical for this CAP.

From the figure, the similarity of the two reflection coefficients at low energies is evident. Specifically, the value of K_{\min} — which has the biggest influence on x_R — is nearly identical between the two. In fact, the optimal values of λ_i from the double-exponential CAP provide a very good initial guess for the optimization of the double-sinh CAP.

Also evident from Fig. 7 is the difference in the two CAPs’ R at high energies. Where the double-exponential R rises back towards unity at high energies, the double-sinh R asymptotes to a value less than unity. This value can be approximately calculated, by considering only the $-i\alpha_2^2/x^2$ behavior of V , to be

$$R \xrightarrow{K \rightarrow \infty} e^{\pi \text{Im} \sqrt{1-4i\lambda_2^2}}, \quad (20)$$

consistent with the limiting behavior found in Ref. [11].

Given the discussion in Sec. III A 2, one might wonder whether allowing the λ_i to be complex — rather than real as assumed so far — could improve the CAPs’ performance even further. The simple answer is that it can. In fact, the double-sinh CAP plotted in Fig. 7 has complex λ_i . We could not, however, find a more optimal double-exponential CAP by allowing λ_i to be complex for the present E_{\min} , E_{\max} , and R_c (see, however, Sec. V B).

Incidentally, Eq. (20) gives the reflection coefficient at *all* energies for a CAP that has the form $-i\alpha_2^2/x^2$ everywhere (see App. D). In particular, the reflection coefficient is not unity at zero energy like the other CAPs we consider and thus corresponds to $K_{\min}=0$. In many ways, such a CAP would be ideal — no optimization would be necessary and λ_2 could simply be calculated by setting Eq. (20) to R_c . Unfortunately, $x_R=110$ a.u. for such a CAP, rendering it uncompetitive with our best CAP — although better than the quadratic CAP often used in the literature (see Table II).

One possible solution would be to simply cut the $-i\alpha_2^2/x^2$ CAP off at some x_0 . Intuitively, this should affect the low-energy behavior of R for wavelengths comparable to and larger than x_0 . The reflection coefficient in this case is again analytic (see App. D), and it can be seen after some exploration that while this expectation is true, R falls off at small k more-or-less like $1/(kx_0)^4$ rather than like the exponential decrease of our best CAPs. Since one chooses x_0 for this CAP from

$$R(k_{\min}x_0) \sim 1/(k_{\min}x_0)^4 = R_c, \quad (21)$$

x_0 — and thus x_R — winds up being large. For instance, $x_R=57$ a.u. for $R_c = 10^{-3}$, which is about double that for our best CAP.

In the context of this discussion, the double-sinh CAP can be seen as providing a smooth cutoff of the $-i\alpha_2^2/x^2$ CAP and similarly leads to modifications of Eq. (20) at small energies.

Fall-to-the-center problem

Whenever an attractive $1/x^2$ potential is used, one must take care to consider the “fall-to-the-center” problem. The real-valued version of such potentials are known [35] to have an infinite number of bound states with energies stretching to $-\infty$ — a fact reflected in the wave function’s oscillating an infinite number of times as $x \rightarrow 0$ — so long as the potential strength exceeds a critical value. This is the quantum-mechanical analog of the classical fall-to-the-center problem in such potentials. Moreover, this effect is possible even for potentials that are only $1/x^2$ for small x like our double-sinh CAP.

No finite numerical representation — such as the grid methods common for TDSE solvers — can represent the infinity of oscillations in the fall-to-the-center regime, and any attempt to accurately represent even a finite number of them will be very costly computationally.

To understand how to avoid this regime, we must examine the small- x behavior of the wave function. From App. D and using its notation, we see that

$$\psi \xrightarrow{z \rightarrow 0} z^{\frac{1}{2} + (a_r - |a_i|)/\sqrt{2}} \exp \left[i \frac{a_r + |a_i|}{\sqrt{2}} \log z \right].$$

This solution assumes $a_r > |a_i|$ and shows that even for a nearly purely imaginary CAP, $a_i=0$, the wave function oscillates an infinity of times as $z \rightarrow 0$. Empirically, choosing $a_r \gg |a_i|$ so that the first term above suppresses the wave function for $z \rightarrow 0$ is sufficient to prevent numerical difficulties. Consequently, we have chosen $a_i=0$, which is equivalent to $\lambda_2^2 = a_r^2 - i/4$.

D. Complex boundary condition

We have so far assumed that the wave function vanishes on the boundary at $x = 0$ as is typical for most

TDSE solvers. But, if the numerical method used to solve the TDSE is flexible enough to allow complex logarithmic boundary conditions, then additional absorption can be built in at very little additional cost.

The effect of the complex boundary condition,

$$\frac{1}{\psi} \frac{d\psi}{dx} = b, \quad (22)$$

can be most easily illustrated for a free particle. If one imposes Eq. (22) at $x=0$ as in Fig. 1, but with no potential, one obtains the reflection coefficient (see App. C for more details, including the effect on bound-state energies)

$$R = \left| \frac{B + iK}{B - iK} \right|^2 \quad (23)$$

with $B = b\beta$. To have absorption, we must have $\text{Im} B \leq 0$; to have maximum absorption, we must have $\text{Re} B = 0$. Thus, setting $B = -iK_0$, we see that $R = 0$ at $K = K_0$. Such a boundary condition therefore makes the boundary perfectly transparent to an incident plane wave of momentum K_0 and partially transparent to other momenta. Moreover, it does so with $x_R = 0$.

Unfortunately, this boundary condition by itself cannot compete with the CAPs since R cannot be made small enough over a large enough energy range. Since implementing it, in principle, requires no change in the spatial grid, though, the possibility of combining it with a CAP and reducing x_R further is worth exploring.

At low energies, the CAP will dominate the behavior of R , and the boundary condition will have little influence. Therefore, one should try to use the boundary condition to modify the high-energy R where it can dominate the behavior. In general, choosing $B \sim -iK_{\text{max}}$ is a good initial guess and allows the reduction of λ —and therefore x_R .

It should be noted that a complex boundary condition cannot be used with the double-sinh CAP due to its singularity at the boundary. Like the centrifugal potential that it resembles, the double-sinh CAP has one regular solution that vanishes at the boundary and one irregular solution that diverges at the boundary [11]. Therefore, it is not possible to form the necessary linear combinations to satisfy Eq. (22).

1. Single-exponential CAP

The reflection coefficient for a single-exponential CAP with a complex boundary condition is again analytic and is given in Eq. (55). The CAP parameters must be re-optimized along with the value of b , and the procedure is largely the same as described above. The fact that K_{min} is essentially unaffected by the addition of the complex boundary condition—so long as $|B| \sim |K_{\text{max}}|$ —simplifies the process.

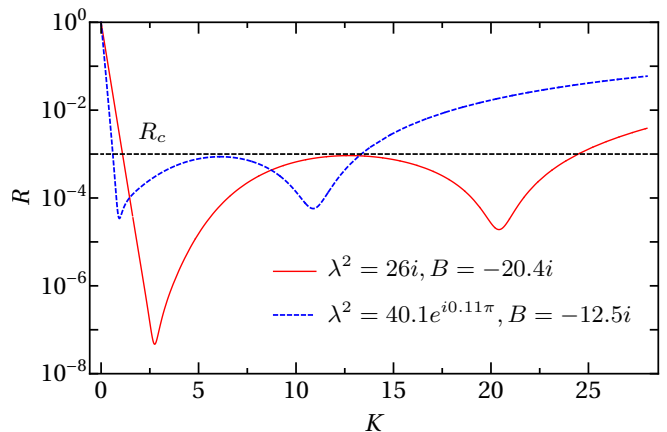


FIG. 8. Reflection coefficient as a function of the unitless momentum for a single-exponential CAP with complex boundary conditions: purely imaginary λ^2 and complex λ^2 .

Examples of optimal choices are shown in Fig. 8 for a purely imaginary CAP and a complex CAP. Comparison with the reflection coefficients shown in Sec. III A shows the effect of the complex boundary condition through the appearance of the high-energy minimum close to $K = |B|$. In both cases, the complex boundary condition has produced a roughly 15% reduction in x_R to 71.7 a.u. and 48.1 a.u., respectively.

2. Double-exponential CAP

Adding a complex boundary condition to the double-exponential CAP also produces an analytic expression for R as given in Eq. (56). Re-optimizing the parameters yields the reflection coefficient shown in Fig. 9. As with the single-exponential CAPs, the boundary condition has introduced a high-energy minimum near $K = |\text{Im} B|$. Unlike the single-exponential CAPs, though, the minimum x_R was found for $\text{Re} B \neq 0$.

This optimum double-exponential CAP continues the pattern that has emerged as we have found improved CAPs: namely, that we add more structure to R and decrease the absorption for the mid-range of K . The double-exponential-CAP reflection coefficients in Fig. 6, for instance, have comparatively little structure—mainly a minimum in R . Moreover, this minimum is relatively broad and orders of magnitude lower than R_c . The R shown in Fig. 9, in contrast, has three narrower minima only one order of magnitude or so lower than R_c .

IV. OPTIMAL CAP

To determine which CAP—among those listed in Table I—is the best, we numerically searched for their optimal parameters, assuming they are purely imaginary po-

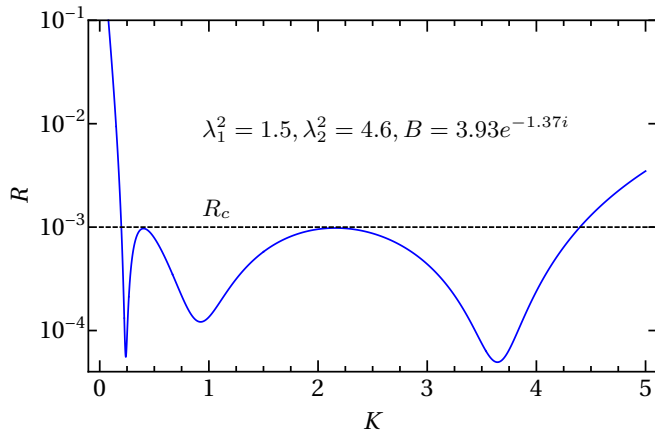


FIG. 9. Optimum reflection coefficient as a function of the unitless momentum for a double-exponential CAP with complex boundary conditions.

tentials. From the discussion above, we know that each could be improved by including a real potential and a complex boundary condition, but we expect — and confirmed with spot tests — that the relative performance of the CAPs will remain qualitatively the same. As mentioned previously, we selected the CAPs to compare based on their apparent popularity in the literature or on the claims made for their performance.

In optimizing these CAPs, we follow the principles described in previous sections that the width of the CAP determines the long-wavelength absorption; and the depth, the short-wavelength. The optimization is then reasonably straightforward once we identify the parameters corresponding to the width and depth.

In Table II, we list the optimal parameters we have found for our E_{\min} , E_{\max} , and R_c . The table includes the resulting values of x_R , and we expect that they are the optimal values to within a few percent. Note that we used $\delta=0.1$ for the M-JWKB CAP based on the solution of $R(E_{\min}) = R_c$ taken from Fig. 3 of Ref. [11]. We show in Fig. 10 the corresponding reflection coefficients.

The cosine masking function should be regarded as a polynomial CAP since its behavior in $0 \leq x \leq x_0$ for the optimal parameters of Table II is largely indistinguishable from the quadratic CAP — thus its x_R is identical to the quadratic CAP. Similarly, for the optimal parameters we found, only the exponential tail of the Pöschl-Teller potential remained on the grid, making its performance essentially identical to that of the purely imaginary single-exponential CAP.

The absorption ranges x_R listed in Table II display a surprisingly large range — more than a factor of 4. Comparing only the purely imaginary potentials, the exponential and Pöschl-Teller forms are more than 30% more efficient than the quadratic CAP. They are also more efficient than the quartic CAP. So, while the exponential form generally seems better, the majority of the dispar-

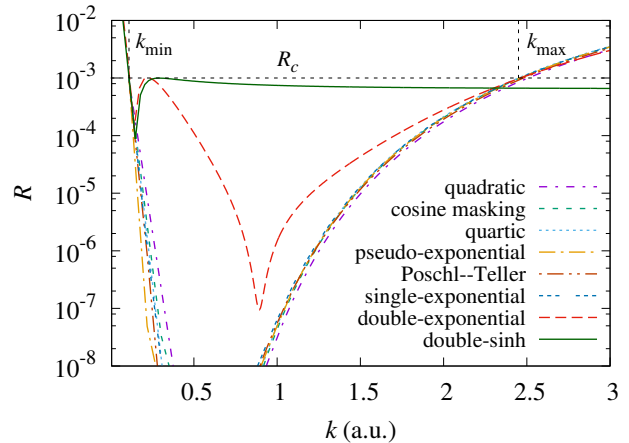


FIG. 10. Optimal reflection coefficients for all CAPs as a function of the electron's momentum using the parameters from Table II. They all satisfy the criteria that $R \leq R_c$ for $0.006 \leq E \leq 3$ a.u., as required.

ity in Table II arises from adding a real part to the CAP and imposing a complex boundary condition.

From Table II, the best performance is found for the double-exponential and double-sinh CAPs, outperforming the next-best CAP — the complex-valued, complex-boundary-condition, single-exponential CAP — by roughly 40%. Compared to the next-best purely imaginary CAP, they hold nearly a factor of 3 advantage in x_R . For reference, we tested the strategy of adding a real part and a complex boundary condition to the quadratic CAP and found x_R shrank only to about 70 a.u. So, while pursuing this strategy with the other CAPs in the table would reduce their x_R , we believe the double-exponential and double-sinh CAPs would remain the best. Interestingly, since the de Broglie wavelength at k_{\min} is 57 a.u., our best CAP manages its efficient absorption in a range of only about half this longest wavelength.

Our recommendation, therefore, is to use the double-sinh CAP when its singularity at the boundary causes no numerical difficulties. In the cases that it does, then the double-exponential CAP is the best choice. The remainder of our discussion will thus focus on these two CAPs.

V. OTHER ABSORPTION CRITERIA

The discussion and optimization so far has centered on the E_{\min} , E_{\max} , and R_c from Eq. (3). Other choices may well be needed, however, for other choices of laser parameters or calculational goals. We thus present in this section the optimal parameters for the double-exponential and double-sinh CAPs for a selection of likely changes in E_{\min} , E_{\max} , and R_c .

TABLE II. Comparison of the optimal absorption ranges for all the CAPs considered. The optimal parameters are given for the electron in our strong-field application — see Eqs. (3) and (4) — so that all quantities are in atomic units.

CAP type	α^2 or (α_1^2, α_2^2)	b	β	x_0	x_R
quadratic	1.21×10^{-5}		—	129	124
cosine masking function	15.9		810	128	124
M-JWKB	—		—	119	118
quartic	2.40×10^{-9}		—	112	95
pseudo-exponential	4.54×10^5		3.27×10^3	240	88
Pöschl-Teller	11.0		20.3	40.0	85
single-exponential	$0.849i$		10.0	—	84
single-exponential+BC	$0.260i$	$-2.04i$	10.0	—	72
single-exponential	$5.24e^{i0.11\pi}$		5.62	—	57
single-exponential+BC	$1.35e^{i0.11\pi}$	$-2.29i$	5.45	—	48
double-exponential	(0.839, 5.09)		1.79	—	30
double-sinh	$(0.298e^{0.104i}, 0.71e^{-0.0906i})$		1.97	—	29
double-exponential+BC	(0.463, 1.42)	$2.19e^{-1.37i}$	1.80	—	28

A. Different energy range

1. Changing E_{\max}

Computationally, the main challenges in solving the TDSE — especially for current and future laser parameters of experimental interest — are that in the course of its strongly-driven dynamics, the electron travels far from the nucleus and gains substantial energy. In particular, we still expect $E_{\max} \propto U_p \propto I/\omega^2$, so that it will grow either with increasing intensity or increasing wavelength — both of which are certainly of interest. While E_{\min} does not change in this case, E_{\max} does, and the CAP must accommodate it.

Under these conditions, the double-sinh CAP from Table II works without change since it has no E_{\max} . In fact, this is its primary advantage. The double-exponential CAP, on the other hand, must be re-optimized for each E_{\max} . As discussed in Sec. II, λ_2 needs the greatest changes — but should have minimal impact on x_R — and these expectations are reflected in the optimal parameters shown in Table III for two longer wavelengths. These parameters were found following the same procedure as above with the same k_{\min} and R_c and with $E_{\max}=10 U_p$ at 10^{14} W/cm². They were found assuming $\psi = 0$ on the boundary, but parameters could certainly be found for a complex boundary condition as well. Note that x_R changes less than about 10% as expected.

2. Changing E_{\min}

In our optimization scheme above, we set E_{\min} to $0.1 \hbar\omega$ for 800-nm light. This choice was motivated by the need to ensure that the entire ionized electron wavepacket is absorbed by the CAP. However, the CAP is often placed at a large distance from the nucleus so that these very slow electrons may not have time to reach the CAP during the propagation. In this case, E_{\min} can be in-

TABLE III. Optimal parameters for the double-exponential CAP for an electron exposed to longer wavelengths. Per the discussion in the text, the only impact of wavelength here is on E_{\max} . All quantities are in atomic units unless otherwise specified.

λ (nm)	E_{\min}	E_{\max}	α_1^2	α_2^2	β	x_R
800	0.006	3	0.839	5.09	1.79	29.9
1600	0.006	8.8	1.07	8.37	1.79	30.7
2400	0.006	20	1.31	12.4	1.79	31.5

creased, thereby decreasing x_R .

Modifications to E_{\min} for the double-sinh CAP are straightforward and do not require re-optimization — again, thanks to the lack of an E_{\max} . Changing k_{\min} just means recalculating β using $\beta = K_{\min}/k_{\min}$ since K_{\min} is fixed. Figure 11 shows the x_R that results as a function of k_{\min} . The figure shows that for modest increases in k_{\min} from our choice in Eq. (4), x_R can be decreased substantially. For example, for k_{\min} above about 0.3 a.u., x_R is smaller than 10 a.u. for $R_c=10^{-3}$. For k_{\min} above about 0.4 a.u., the x_R for $R_c=10^{-10}$ is equal to or smaller than the original $x_R=28.8$ a.u. for the double-sinh CAP.

For a double-exponential CAP, it is still true that the larger k_{\min} , the smaller λ_1 and λ_2 , and the smaller x_R . However, re-optimization is required to obtain the smallest x_R . For instance, if one can accept doubling k_{\min} to 0.22 a.u., then we can have

$$\lambda_1^2 = 2.00 \text{ and } \lambda_2^2 = 9.11, \text{ so that } x_R = 17.0 \text{ a.u.} \quad (24)$$

with $\beta=0.90$ a.u.

On the other hand, the double-exponential CAP can be adjusted just like the double-sinh CAP if a less-than-optimal x_R can be tolerated. Specifically, the values of λ_i^2 can be kept, so that K_{\min} does not change, and β can be recalculated from $\beta = K_{\min}/k_{\min}$. In this case, k_{\max} grows to $k_{\min}K_{\max}/K_{\min}$, guaranteeing absorption at the prescribed level beyond E_{\max} . The resulting x_R

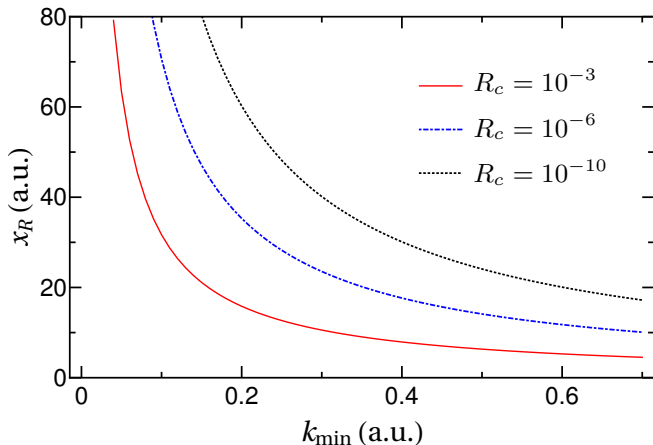


FIG. 11. Absorption range x_R as a function of k_{\min} for the double-sinh CAP. The parameters for $R_c \leq 10^{-3}$ can be found in Table IV.

looks very much like those in Fig. 11, except that x_R for $R_c=10^{-3}$ does not go below 10 a.u. until $k_{\min}=0.45$ a.u. For comparison, $x_R=17.4$ a.u. at $k_{\min}=0.22$ a.u. and is thus slightly worse than the fully re-optimized result in Eq. (24).

B. Different R_c

One of the primary design goals of a CAP is to leave the physical wave function—the wave function outside the absorption region—unaffected. Of course, this goal can only be achieved to a given accuracy, and that accuracy is controlled by R_c . To see the relation, consider the physical wave function written in Fig. 1 from which R is extracted,

$$\psi(x) = e^{-ikx} + \sqrt{R}e^{i\varphi}e^{ikx}, \quad x \geq x_R. \quad (25)$$

The second term is precisely the unwanted contribution from reflection, and it is limited by $R \leq R_c$ by design. Given that this is just one component of the time-dependent wave function, this error is always relative to the first term. In other words, if one desires n digits to be accurate, then one should choose $R_c=10^{-2n}$.

We thus provide in Table IV the optimal parameters for the double-exponential and double-sinh CAPs with $\psi=0$ on the boundary, assuming $E_{\min}=0.006$ a.u. and $E_{\max}=3$ a.u. as before, for several smaller R_c . These results show that the absorption range for each type of CAP is comparable, with the double-sinh CAP tending to be a few percent smaller. Qualitatively, the reflection coefficients as a function of K resemble those shown previously for $R_c=10^{-3}$. As with the other CAP parameters we have given, we expect these to produce x_R within a few percent of the global optimum.

Note that the probability density corresponding to the wave function in Eq. (25),

$$|\psi(x)|^2 = 1 + R + 2\sqrt{R}\cos(2kx + \varphi), \quad (26)$$

can be useful for diagnosing issues with the CAP in a time-dependent calculation. In particular, the last term above is the source of the telltale ripples in the probability density near the edge of a grid. The ripples' size is limited by $\sqrt{R_c}$ and identifying their wavelength via Eq. (26) in a time-dependent wave function reveals the offending energy.

VI. TIME-DEPENDENT DEMONSTRATION

To verify that the improved performance of our recommended CAPs does indeed carry over to the time-dependent problem and its numerical solution, we solve the TDSE for free-electron wavepacket propagation. The wavepacket we use possesses a broad momentum distribution comparable to the target momentum range from Eq. (4), as shown in Fig. 12(a).

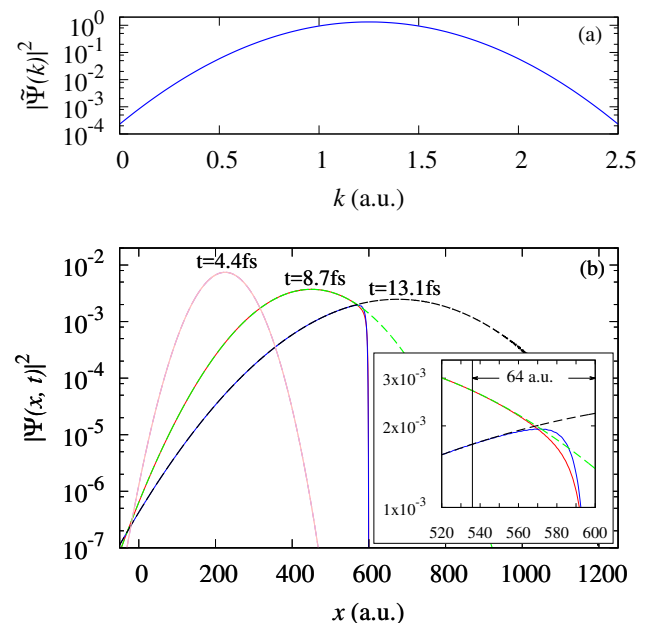


FIG. 12. (a) Momentum distribution of the free wavepacket, covering $0.11 \leq k \leq 2.45$ a.u. (b) Demonstration of the $R_c=10^{-6}$ double-sinh CAP using a free wavepacket. Solid lines show the with-CAP wavepacket, calculated for $-600 \text{ a.u.} \leq x \leq 600 \text{ a.u.}$; and dashed lines, the without-CAP wavepacket, calculated for $-600 \text{ a.u.} \leq x \leq 1200 \text{ a.u.}$ Inset: Expanded view of the absorption region $536 \text{ a.u.} \lesssim x \leq 600 \text{ a.u.}$ for clearer comparison.

We again use FEDVR as the spatial representation and propagate the wave function using the short-time evolution operator

$$\psi(x, t + \delta) = e^{-iH\delta}\psi(x, t) \quad (27)$$

TABLE IV. Optimal parameters for double-exponential and double-sinh CAPs for $R_c \leq 10^{-3}$.

Double exponential					Double sinh			
λ_1^2	λ_2^2	β (a.u.)	x_R (a.u.)	R_c	x_R (a.u.)	λ_1^2	λ_2^2	β (a.u.)
2.69	16.3	1.79	29.9	10^{-3}	28.8	$1.16e^{0.104i}$	$2.75 - 0.25i$	1.97
$4.83e^{0.187i}$	$31e^{0.0968i}$	2.77	44.7	10^{-4}	40.4	$1.78e^{0.23i}$	$4.30 - 0.25i$	2.90
$7.21e^{0.0486i}$	$57.6e^{-0.411i}$	3.38	54.5	10^{-5}	52.6	$2.66e^{0.346i}$	$6.82 - 0.25i$	3.87
$16.1e^{-0.219i}$	80.0	4.02	68.4	10^{-6}	64.2	$3.8e^{0.36i}$	$9.67 - 0.25i$	4.77
$19.4e^{i0.135\pi}$	$141e^{-0.073i}$	6.64	102	10^{-8}	89.4	$6.75e^{0.46i}$	$17.2 - 0.25i$	6.77
$30.8e^{i0.132\pi}$	$232e^{-0.204i}$	8.48	130	10^{-10}	109	$11.85e^{0.14i}$	$26.9 - 0.25i$	8.02
48	$355e^{-0.328i}$	9.04	144	10^{-12}	132	$16.1e^{0.21i}$	$38.7 - 0.25i$	9.77

where the Hamiltonian includes the CAP $V(x)$,

$$H = H_0 + V, \quad (28)$$

and H_0 is merely the kinetic energy in the present case. We evaluate $e^{-iH\delta}$ using the split-operator form [36]

$$e^{-iH\delta} \approx e^{-iV\frac{\delta}{2}} e^{-iH_0\delta} e^{-iV\frac{\delta}{2}}. \quad (29)$$

Since V is diagonal in FEDVR, $e^{-iV\delta/2}$ can be easily evaluated and applied. Moreover, in this form, the singularity in the double-sinh CAP causes no problems whatsoever. The action of the remaining term in H_0 is calculated via a Padé approximation [37].

Equation (29) is a simple and convenient way to add a CAP to any propagator. In many cases, the alternative, keeping the CAP in H , would require modifications of the propagation algorithm or parameters to handle its non-Hermiticity or the singularity of the double-sinh CAP—or both. These issues were discussed somewhat in Sec. III C and more in Ref. [11]. Using Eq. (29) avoids these concerns and is more than sufficient for the application of the CAP.

The FEDVR element distribution is uniform in the range $-600 \text{ a.u.} \leq x \leq 1200 \text{ a.u.}$, and we require $\psi = 0$ at the boundaries. Given that the wavepacket is initially centered near $x = 0$, this box is large enough for the wavepacket to propagate for 10 fs without significant reflection at the boundaries even without CAPs. This will be our reference solution. We carry out a second, identical propagation but apply the double-sinh CAP at $536 \text{ a.u.} \lesssim x \leq 600 \text{ a.u.}$. For this example, we choose the CAP designed to have $R_c = 10^{-6}$ using the parameters shown in Table IV. We thus compare the wavepacket with and without applying the CAP. All the results have been tested to be converged to at least 3 digits with respect to all numerical parameters.

Figure 12 shows the two wavepackets at different times. It is clear that the CAP is performing as expected since the wavepacket decays in the absorbing region without any of the characteristic oscillations of reflections visible—at least without enlarging the plot by a factor of four or five. For comparison, the wavepacket without a CAP equally clearly shows the reflection oscillations at $t=13.1 \text{ fs}$ for reflections from the boundary at $x=1200 \text{ a.u.}$

In addition, the with-CAP wavepacket is numerically unaffected before entering the absorbing region, agreeing with the without-CAP wavepacket to at least 3 digits for $x \lesssim 536 \text{ a.u.}$ for all times, even as more than 70% of the wavepacket has been absorbed. This agreement shows that the absorption range x_R defined in the time-independent study is consistent with the results from the time-dependent propagation.

Enlarging Fig. 12 by a factor of at least four or five will reveal the tiny reflection ripples in the with-CAP wavepacket near and in the absorption region. Their relative magnitude is about $10^{-3} = \sqrt{R_c}$ as expected. Per the discussion in Sec. V B, such oscillations are unavoidable with a CAP and testing with other CAPs and values of R_c further support the conclusions there. For example, the oscillation for $R_c=10^{-3}$ becomes fairly noticeable, which suggests that R_c should in practice be no larger than 10^{-4} —*i.e.*, two digits in the wave function—to provide quantitatively reliable results. Finally, we note that the roughly 15-fs propagation time is comparable to a typical strong-field calculation, bringing some realism to this simple demonstration.

VII. SUMMARY

We have presented a systematic study to boost the performance of complex absorbing potentials. Based on the time-independent reflection coefficient, we were able to quantitatively design the most optimal absorbing potential of a given form. In particular, for ultrafast, strong-field TDSE solvers, the optimal CAP parameters should be determined by the absorbing energy range required for the laser parameters and by the desired accuracy of the TDSE solutions.

We proposed two new CAPs—namely, the double-sinh CAP and the double-exponential CAP—that significantly outperform the CAPs currently in standard use. Their superiority was demonstrated through comparison with optimized versions of most of the CAPs commonly found in the literature. Both of our proposed CAPs overcome the primary impediment to efficient performance—absorption of long wavelengths—while also absorbing a large range of energies that covers basically all strong-

field processes. Because we quantified the CAP's performance and identified x_R as the figure of merit for their efficiency, we could show that using an exponential CAP already improved on the common quadratic CAP's performance by one third. A further factor of almost three was gained, however, by adding a real part to the CAP — a strategy well known in other uses of CAPs, but not in strong-field applications.

We highly recommend the double-sinh CAP for local spatial representations, such as FEDVR where the potential is diagonal. It is efficient, easy to use, and easy to adapt to different absorption criteria — i.e., energy range and level of absorption. Incorporating it into the time propagation via split-operator methods is easy and effective.

For other spatial representations, the double-sinh and the double-exponential CAPs are equally recommended. However, care might need to be taken for the double-sinh singularity close to the boundary. In case the double-sinh singularity is a problem for the propagator, the double-exponential CAP should be chosen. Although optimization of the double-exponential CAP is more involved than for the double-sinh CAP, it is still fairly straightforward. Its optimization procedure, along with that for the double-sinh CAP, is detailed in this work.

Appendix A REFLECTION COEFFICIENT FOR SINGLE-EXPONENTIAL CAP

We start from the Schrödinger equation for the single-exponential CAP:

$$\left[-\frac{\hbar^2}{2m} \frac{d^2}{dx^2} - \frac{\alpha^2 \hbar^2}{2m} e^{-x/\beta} \right] \psi = E\psi = \frac{\hbar^2 k^2}{2m} \psi. \quad (30)$$

Setting $z = x/\beta$ gives

$$\left[-\frac{d^2}{dz^2} - \lambda^2 e^{-z} \right] \psi = K^2 \psi, \quad (31)$$

where $\lambda \equiv \alpha\beta$ and $K \equiv k\beta$. We define

$$\xi = 2\lambda e^{-z/2},$$

so that Eq. (31) becomes

$$\left[\xi^2 \frac{d^2}{d\xi^2} + \xi \frac{d}{d\xi} + \xi^2 + 4K^2 \right] \psi = 0. \quad (32)$$

This is Bessel's equation; the general solution is thus

$$\psi = C J_{2iK}(\xi) + D J_{-2iK}(\xi). \quad (33)$$

To obtain the reflection coefficient, we need C and D and we need to analyze the asymptotic behavior of these solutions. Starting with the latter, the $z \rightarrow \infty$ ($x \rightarrow \infty$) behavior can be found from the $\xi \rightarrow 0$ expansions,

$$\begin{aligned} J_{2iK}(\xi) &\xrightarrow{z \rightarrow \infty} \frac{\lambda^{2iK}}{\Gamma(1+2iK)} e^{-iKz} \\ J_{-2iK}(\xi) &\xrightarrow{z \rightarrow \infty} \frac{\lambda^{-2iK}}{\Gamma(1-2iK)} e^{iKz}. \end{aligned} \quad (34)$$

To find C and D , we impose the $x = 0$ boundary condition,

$$\psi(x=0) = \psi(z=0) = \psi(\xi=2\lambda) = 0. \quad (35)$$

Thus,

$$D = -\frac{J_{2iK}(2\lambda)}{J_{-2iK}(2\lambda)} C. \quad (36)$$

Finally, the asymptotic solution reads

$$\psi \xrightarrow{z \rightarrow \infty} C \left[\frac{\lambda^{2iK}}{\Gamma(1+2iK)} e^{-iKz} - \frac{\lambda^{-2iK}}{\Gamma(1-2iK)} \frac{J_{2iK}(2\lambda)}{J_{-2iK}(2\lambda)} e^{iKz} \right]. \quad (37)$$

From this expression, the reflection coefficient can be found to be

$$R = e^{4K \arg \lambda^2} \left| \frac{J_{2iK}(2\lambda)}{J_{-2iK}(2\lambda)} \right|^2. \quad (38)$$

Note that if λ is real, then $R \equiv 1$ as it should with no absorption.

Appendix B REFLECTION COEFFICIENT FOR DOUBLE-EXPONENTIAL CAP

As in App. A, we start from a unitless Schrödinger equation,

$$\left[-\frac{d^2}{dz^2} - \lambda_1^2 e^{-z/2} - i\lambda_2^2 e^{-z} \right] \psi = K^2 \psi. \quad (39)$$

with

$$z = \frac{x}{\beta} \quad \lambda_1 = \alpha_1 \beta \quad \lambda_2 = \alpha_2 \beta \quad K = k\beta. \quad (40)$$

We assume both λ_i are real, making the longer-range potential real in accord with the discussion in the text. That is, the real potential accelerates the wave before it encounters the absorbing potential.

Defining

$$\xi = 2\lambda_2 e^{-z/2} \quad \text{and} \quad A = \frac{\lambda_1^2}{\lambda_2}, \quad (41)$$

we get

$$\left[\xi^2 \frac{d^2}{d\xi^2} + \xi \frac{d}{d\xi} + 2A\xi + i\xi^2 + 4K^2 \right] \psi = 0 \quad (42)$$

This form of the equation makes clear the motivation for our choice of potential: having one potential being the square of the other (in form) produces the polynomial in ξ seen in the equation. Since the polynomial is quadratic, the equation has analytic solutions.

Setting $\gamma = e^{i\pi/4}$ and $\eta = \frac{1}{2} - \gamma\Lambda$, the solution can be written as

$$\psi = e^{\gamma^3 \xi + 2iK \ln \xi} \left[C U(\eta + 2iK, 1 + 4iK, -2\gamma^3 \xi) + D L_{-\eta - 2iK}^{4iK}(-2\gamma^3 \xi) \right], \quad (43)$$

where U and L are the confluent hypergeometric and Laguerre functions, respectively.

Analyzing the asymptotic behavior, we have

$$\begin{aligned} e^{\gamma^3 \xi + 2iK \ln \xi} U &\xrightarrow{z \rightarrow \infty} \frac{(2\lambda_2)^{2iK} \Gamma(-4iK)}{\Gamma(\eta - 2iK)} e^{-iKz} \\ &\quad + \frac{(2\lambda_2)^{-2iK} 2^{-4iK} e^{-\pi K} \Gamma(4iK)}{\Gamma(\eta + 2iK)} e^{iKz} \\ e^{\gamma^3 \xi + 2iK \ln \xi} L &\xrightarrow{z \rightarrow \infty} (2\lambda_2)^{2iK} L_{-\eta - 2iK}^{4iK}(0) e^{-iKz}. \end{aligned} \quad (44)$$

The boundary condition $\psi(x=0) = 0$ gives

$$D = -\frac{U(\eta + 2iK, 1 + 4iK, -4\lambda_2 \gamma^3)}{L_{-\eta - 2iK}^{4iK}(-4\lambda_2 \gamma^3)} C. \quad (45)$$

The reflection coefficient can now be extracted, and a little algebra applied, to give

$$R = \left| \frac{{}_1F_1(\eta + 2iK, 1 + 4iK, -4\gamma^3 \lambda_2)}{{}_1F_1(\eta - 2iK, 1 - 4iK, -4\gamma^3 \lambda_2)} \right|^2. \quad (46)$$

For a purely real V (*i.e.*, $\lambda_2 \rightarrow 0$), we recover $R = 1$ as we should. For $\lambda_1 = 0$, R reduces to the single-exponential expression Eq. (38) with λ purely imaginary.

Appendix C COMPLEX BOUNDARY CONDITION

A Zero potential

It is easiest to understand the effect of the complex boundary condition (b is complex)

$$\frac{1}{\psi} \frac{d\psi}{dx} = b \quad (47)$$

from the free-particle equation

$$-\frac{d^2}{dz^2} \psi = K^2 \psi \quad (48)$$

in the same unitless notation as in the previous appendices. In this notation, we must require

$$\frac{1}{\psi} \frac{d\psi}{dz} = B, \quad (49)$$

where $B = b\beta$. The solution is, as usual,

$$\psi = C e^{iKz} + D e^{-iKz}. \quad (50)$$

When combined with the boundary condition, one finds

$$R = \left| \frac{B + iK}{B - iK} \right|^2. \quad (51)$$

As discussed in the text, this R goes to zero at $K = K_0$ when $B = -iK_0$. Physically, this condition corresponds to setting an outgoing-wave boundary condition (on the left boundary) for an incident momentum K_0 . The boundary is thus perfectly transparent at this momentum, but imperfectly so at other momenta.

B Effect on bound states

It is natural to ask what effect such a boundary condition might have on the energies of any bound states in the system. One general way to answer this question is to consider an arbitrary potential at $z = 0$ and write

$$\psi = \begin{cases} AF(z) & z \leq z_0 \\ Ce^{-\kappa(z-z_0)} + De^{\kappa(z-z_0)} & z > z_0 \end{cases} \quad (52)$$

with $\kappa = \beta\sqrt{2m|E|/\hbar^2}$ and $F(z)$ the energy-dependent solution appropriate to the arbitrary potential satisfying the required boundary condition at $z = 0$. Although this specific description assumes a short-range potential, a similar argument can be made for the Coulomb potential.

The wave function in Eq. (52) must satisfy the log-derivative boundary condition from Eq. (49) at $z = z_1$ — this is why the exponentially-growing solution must be retained. Imposing this boundary condition leads to the following transcendental equation for the energy of the bound state:

$$F'(z_0) + \kappa F(z_0) = \frac{B + \kappa}{B - \kappa} [F'(z_0) - \kappa F(z_0)] e^{-2\kappa(z_1 - z_0)}. \quad (53)$$

This equation should be compared with the physical quantization condition

$$F'(z_0) + \kappa F(z_0) = 0, \quad (54)$$

to which Eq. (53) reduces in the $z_1 \rightarrow \infty$ limit as it should.

Since in any practical numerical solution of the TDSE the boundary of the numerical grid must be large compared to the size of the bound state, we will have $z_1 \gg z_0$. Therefore, so long as $B - \kappa \neq 0$, the exponential term on the right-hand-side of Eq. (53) will dominate — and thus make Eq. (53) a very good approximation to Eq. (54) — guaranteeing that the real part of the energy found with the complex boundary condition will be very close to the physical energy. To be sure, it will acquire a small imaginary part reflecting the decay of the ground state due to the complex boundary condition, but it should be completely negligible.

This result for the bound-state energies is completely consistent with the intuitive notion that the effect of the

complex boundary condition—indeed the CAPs, too—on the bound states should be negligible so long as the bound-state wave function is vanishingly small at the boundary $z = z_1$ (or in the absorbing region of the CAP).

C Single- and double-exponential CAPs

The reflection coefficient for the single-exponential CAP with a complex boundary condition is still analyt-

ical. It is found by imposing Eq. (49) on the general solution for the single-exponential CAP from Eq. (33). After a little algebra, one obtains

$$R = e^{4K \arg \lambda^2} \left| \frac{(B + iK)J_{2iK}(2\lambda) - \lambda J_{1+2iK}(2\lambda)}{(B - iK)J_{-2iK}(2\lambda) - \lambda J_{1-2iK}(2\lambda)} \right|^2. \quad (55)$$

The same procedure can be carried out for the double-exponential CAP using the general solution from Eq. (43) to find

$$R = \left| \frac{(B + iK + \gamma^3 \lambda_2) {}_1F_1(\eta + 2iK, 1 + 4iK, -4\gamma^3 \lambda_2) - 2\gamma^3 \lambda_2 (\eta + 2iK) {}_1F_1(\eta + 2iK + 1, 2 + 4iK, -4\gamma^3 \lambda_2) / (1 + 4iK)}{(B + iK + \gamma^3 \lambda_2) {}_1F_1(\eta - 2iK, 1 - 4iK, -4\gamma^3 \lambda_2) - 2iK {}_1F_1(\eta - 2iK, -4iK, -4\gamma^3 \lambda_2)} \right|^2. \quad (56)$$

Note that both Eq. (55) and Eq. (56) reduce to the reflection coefficient with $\psi = 0$ in the $B \rightarrow \infty$ limit as they should.

Appendix D REFLECTION COEFFICIENT FOR $-i\alpha_2^2/x^2$ CAP

We start from the Schrödinger equation

$$\left[-\frac{\hbar^2}{2m} \frac{d^2}{dx^2} - \frac{\hbar^2}{2m} \frac{ia^2 + \frac{1}{4}}{x^2} \right] \psi = \frac{\hbar^2}{2m} k^2 \psi. \quad (57)$$

Defining $z = kx$, we must solve

$$\left[-\frac{d^2}{dz^2} - \frac{ia^2 + \frac{1}{4}}{z^2} \right] \psi = \psi. \quad (58)$$

The general solution is

$$\psi = \sqrt{z} \left[C J_{a/\gamma}(z) + D J_{-a/\gamma}(z) \right] \quad (59)$$

with $\gamma = e^{i\pi/4}$ as before. Since we require $\psi(0) = 0$, we need the small- z behavior of the Bessel functions

$$J_\nu(z) \xrightarrow{z \rightarrow 0} \frac{1}{\Gamma(1 + \nu)} \left(\frac{z}{2} \right)^\nu. \quad (60)$$

For the general case of complex a , $a = a_r + ia_i$, one can show that requiring the real part of the potential to be attractive and the imaginary part to be absorbing leads to

$$a_r > 0 \text{ and } a_i < 0 \text{ with } |a_r| > |a_i|. \quad (61)$$

These conditions, together with Eq. (60), require us to set $D = 0$.

Finally, using the large- z behavior of the Bessel function,

$$\sqrt{z} J_{a/\gamma}(z) \xrightarrow{z \rightarrow \infty} \sqrt{\frac{2}{\pi}} \cos \left(\frac{\pi}{4} + \frac{a\pi}{2\gamma} - z \right), \quad (62)$$

allows us to extract the reflection coefficient,

$$R = e^{-\sqrt{2}\pi(a_r - a_i)}. \quad (63)$$

Keeping in mind that $a_i < 0$ under the conditions we have assumed, this equation shows that both the real and imaginary parts of the CAP contribute to decreasing the final absorption. We also see that this equation is identical to Eq. (20) once the conversion from a to λ_2 is made.

Effect of truncation

If we are willing to sacrifice the energy independence of R at small energies by truncating the CAP at x_0 ,

$$V = \begin{cases} -\frac{\hbar^2}{2m} \frac{ia^2 + \frac{1}{4}}{x^2} & x \leq x_0 \\ 0 & x > x_0 \end{cases}, \quad (64)$$

then one can again obtain an analytic expression for the reflection coefficient.

The wave function is

$$\psi = \begin{cases} AF(z) & z \leq z_0 \\ Ce^{-i(z-z_0)} + De^{i(z-z_0)} & z > z_0 \end{cases} \quad (65)$$

with $z_0 = kx_0$ and $F(z) = \sqrt{z} J_{a/\gamma}(z)$. The reflection coefficient is thus

$$R = \left| \frac{D}{C} \right|^2 = \left| \frac{F(z_0) - iF'(z_0)}{F(z_0) + iF'(z_0)} \right|^2. \quad (66)$$

The notation F' indicates a derivative with respect to z , $F' = dF/dz$, and the log-derivative of F at z_0 is

$$\left. \frac{F'}{F} \right|_{z=z_0} = \frac{1 - 2a/\gamma}{2z_0} + \frac{J_{a/\gamma-1}(z_0)}{J_{a/\gamma}(z_0)}. \quad (67)$$

A plot of the reflection coefficient from Eq. (66) looks qualitatively like the double-sinh reflection coefficients

in Figs. 7 and 10. However, instead of falling exponentially with k at small k , it falls more slowly—like $1/z_0^4 = 1/(kx_0)^4$. In addition, because of the sharp cutoff in the potential, R oscillates in z_0 with minima separated by π at positions corresponding roughly to

$$z_0 = kx_0 = n\pi.$$

ACKNOWLEDGMENTS

This work is supported by the Chemical Sciences, Geoscience, and Biosciences Division, Office for Basic Energy Sciences, Office of Science, U.S. Department of Energy.

-
- [1] R. Heather and H. Metiu, *The Journal of Chemical Physics* **86**, 5009 (1987), <http://dx.doi.org/10.1063/1.452672>.
- [2] L. Tao and A. Scrinzi, *New Journal of Physics* **14**, 013021 (2012).
- [3] F. Morales, T. Bredtmann, and S. Patchkovskii, *Journal of Physics B: Atomic, Molecular and Optical Physics* **49**, 245001 (2016).
- [4] R. Kosloff and D. Kosloff, *Journal of Computational Physics* **63**, 363 (1986).
- [5] A. Vibok and G. G. Balint-Kurti, *The Journal of Chemical Physics* **96**, 7615 (1992).
- [6] A. Vibok and G. G. Balint-Kurti, *The Journal of Physical Chemistry* **96**, 8712 (1992).
- [7] D. Macias, S. Brouard, and J. Muga, *Chemical Physics Letters* **228**, 672 (1994).
- [8] U. V. Riss and H. Meyer, *The Journal of Chemical Physics* **105**, 1409 (1996).
- [9] J.-Y. Ge and J. Z. H. Zhang, *The Journal of Chemical Physics* **108**, 1429 (1998).
- [10] A. N. Hussain and G. Roberts, *Phys. Rev. A* **63**, 012703 (2000).
- [11] D. E. Manolopoulos, *The Journal of Chemical Physics* **117**, 9552 (2002), <http://dx.doi.org/10.1063/1.1517042>.
- [12] B. Poirier and T. Carrington, *The Journal of Chemical Physics* **119**, 77 (2003).
- [13] J. Muga, J. Palao, B. Navarro, and I. Egusquiza, *Physics Reports* **395**, 357 (2004).
- [14] M. Tarana and C. H. Greene, *Phys. Rev. A* **85**, 013411 (2012).
- [15] V. V. Strelkov, M. A. Khokhlova, A. A. Gonoskov, I. A. Gonoskov, and M. Y. Ryabikin, *Phys. Rev. A* **86**, 013404 (2012).
- [16] L. Yue and L. B. Madsen, *Phys. Rev. A* **88**, 063420 (2013).
- [17] P. Krause, J. A. Sonk, and H. B. Schlegel, *The Journal of Chemical Physics* **140**, 174113 (2014).
- [18] J. L. Krause, K. J. Schafer, and K. C. Kulander, *Phys. Rev. A* **45**, 4998 (1992).
- [19] T. N. Rescigno, M. Baertschy, W. A. Isaacs, and C. W. McCurdy, *Science* **286**, 2474 (1999).
- [20] T. N. Rescigno and C. W. McCurdy, *Phys. Rev. A* **62**, 032706 (2000).
- [21] F. He, C. Ruiz, and A. Becker, *Phys. Rev. A* **75**, 053407 (2007).
- [22] L. Tao, W. Vanroose, B. Repts, T. N. Rescigno, and C. W. McCurdy, *Phys. Rev. A* **80**, 063419 (2009).
- [23] A. Scrinzi, *Phys. Rev. A* **81**, 053845 (2010).
- [24] E. Y. Sidky and B. D. Esry, *Phys. Rev. Lett.* **85**, 5086 (2000).
- [25] A. Hamido, J. Eiglsperger, J. Madroñero, F. Mota-Furtado, P. O'Mahony, A. L. Frapiccini, and B. Piraux, *Phys. Rev. A* **84**, 013422 (2011).
- [26] H. Miyagi and L. B. Madsen, *Phys. Rev. A* **93**, 033420 (2016).
- [27] J. Z. H. Zhang, *The Journal of Chemical Physics* **92**, 324 (1990), <http://dx.doi.org/10.1063/1.458433>.
- [28] C. J. Williams, J. Qian, and D. J. Tannor, *The Journal of Chemical Physics* **95**, 1721 (1991), <http://dx.doi.org/10.1063/1.461022>.
- [29] G. H. Yao and S. I. Chu, *Chem. Phys. Lett.* **198**, 39 (1992).
- [30] S. Yoshida, S. Watanabe, C. O. Reinhold, and J. Burgdörfer, *Phys. Rev. A* **60**, 1113 (1999).
- [31] C. W. McCurdy, D. A. Horner, and T. N. Rescigno, *Phys. Rev. A* **63**, 022711 (2001).
- [32] B. I. Schneider, L. A. Collins, and S. X. Hu, *Phys. Rev. E* **73**, 036708 (2006).
- [33] M. Aymar, C. H. Greene, and E. Luc-Koenig, *Rev. Mod. Phys.* **68**, 1015 (1996).
- [34] G. Pöschl and E. Teller, *Zeitschrift für Physik* **83**, 143 (1933).
- [35] L. D. Landau and E. M. Lifshitz, *Quantum Mechanics: Non-Relativistic Theory* (Pergamon Press, 1977).
- [36] B. I. Schneider, J. Feist, S. Nagele, R. Pazourek, S. Hu, L. A. Collins, and J. Burgdörfer, in *Quantum Dynamic Imaging: Theoretical and Numerical Methods*, edited by A. D. Bandrauk and M. Ivanov (Springer Science & Business Media, 2011).
- [37] S. Blanes, F. Casas, J. Oteo, and J. Ros, *Physics Reports* **470**, 151 (2009).